Supplementary Information for

Controlled coaggregation pathways of perovskite nanocrystals and supramolecular dye assemblies

Naoki Kubo[1], Mitsuaki Yamauchi[2]*, Naoki Aratani[3], Hiroko Yamada[2], and Sadahiro Masuo[1]*

[1]Department of Applied Chemistry for Environment, Kwansei Gakuin University, 1 Gakuen, Uegahara, Sanda, Hyogo 669-1330 (Japan). [2]Institute for Chemical Research, Kyoto University, Gokasho, Uji, Kyoto 611-0011 (Japan). [3]Division of Materials Science, Nara Institute of Science and Technology, 8916-5 Takayama-cho, Ikoma 630-0192 (Japan).

Table of Contents

1. Materials and Methods

Materials: Column chromatography separations were performed using silica gel 60 N (spherical, neutral, particle size 63–210 μm; Kanto Chemical). All commercially available reagents and were of reagent grade and were used without purification. The solvents for measurements were all of spectral grade and were used without purification.

General methods: ^{1}H nuclear magnetic resonance (NMR) spectra were recorded on a JEOL JNM ECX-500II NMR spectrometer, and the chemical shifts are reported in ppm (δ) with the signal of TMS ($\delta = 0$) as the internal standard. High-resolution mass spectra (HRMS) were obtained with a JEOL SpiralTOF JMS-S3000 spectrometer (MALDI-TOF) using a positive ionization mode. UV/Vis absorption and photoluminescence (PL) spectra were recorded on a SHIMADZU UV-3600 spectrophotometer and a HITACHI F-7000 spectrophotometer, respectively. Absolute PL quantum yield (PLQY) was estimated on a HAMAMATSU Quantaurus-QY Plus C13534-01 with an integrating sphere. Fourier transform infrared (FTIR) spectra were recorded on a JASCO FT/IR-4600 spectrometer. The samples were prepared on the CaF_2 substrate (thickness 3 mm).

Computational method: The calculation of a PBI derivative was carried out with the Gaussian 16 package using the density functional theory (DFT) method with the B3LYP hybrid functional. The structures were optimized using the DFT (ground state) method with a 6-31G + (d,p) basis set (# opt freq b3lyp/6-31+g(d,p) geom=connectivity fchec). The calculation was performed in the gas phase.

AFM observation: Atomic force microscopy (AFM) images were acquired under ambient conditions using NanoWizard II (JPK Instruments) with an OMCL-AC160TS-R3 cantilever. The samples were prepared by spin-coating solutions onto clean coverslip.

2. Synthesis and Characterization of PBI derivatives

2-1. DFT calculations of a PBI derivative

Supplementary Figure 1. Molecular conformation of the PBI core unit of **PBI$_c$** obtained by DFT calculations. *N*-Alkyl chains were replaced by methyl groups.

2-2. Synthesis and characterization of PBI$_c$

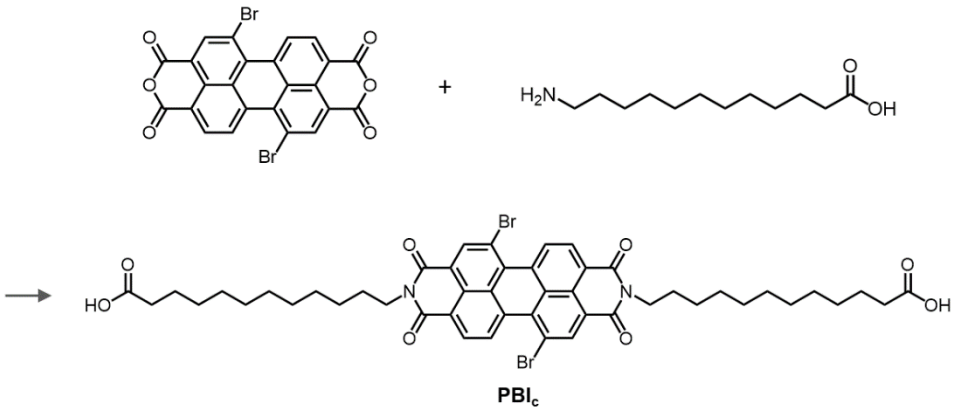

Scheme 1. Synthesis of **PBI$_c$**. Condition: NMP, toluene, 65 ℃, 4 hours.

PBI$_c$ was synthesized according to the reported method with minor modifications.[1] First, 1,7-dibromo-3,4,9,10-tetracarboxylic acid dianhydride (100 mg, 0.18 mmol), 12-aminolauric acid (86 mg, 0.4 mmol) and *N*-methyl-2-pyrrolidone (NMP, 3 mL) were added to a flask. The mixture was stirred at room temperature for 30

minutes, and then stirred at 65 °C for another 60 minutes. After that, toluene (1 mL) was added into the solution and the reaction mixture was stirred for 3 hours at 65 °C. After cooling, methanol (15 mL) was added into the reaction mixture, and the resulting suspension was separated by centrifugation (15000 rpm, 10 min, 25 °C). The resulting dark red solid was purified by column chromatography on silica gel ($CHCl_3$:methanol = 10:1, Rf = 0.27) and reprecipitated ($CHCl_3$/methanol) to give **PBI$_c$** (18 mg, 11% yield). ^{1}H NMR (500 MHz, $CDCl_3$, 50 °C): δ (ppm) = 9.51 (d, J = 8.2 Hz, 2H), 8.93 (s, 2H), 8.71 (d, J = 8.3 Hz, 2H), 4.24 (t, J = 7.5 Hz, 4H), 2.29 (t, J = 7.5 Hz, 4H), 1.80–1.75 (m, 4H), 1.62–1.56 (m, 4H), 1.47–1.26 (m, 28H), as shown in Supplementary Figure 2. The ^{13}C NMR spectrum could not be measured due to poor solubility. HRMS (MALDI-TOF, DCTB matrix, TFANa): m/z $[M+Na]^+$ calcd for $C_{48}H_{52}Br_2N_2O_8Na$ 965.1983, observed 965.1979, as shown in Supplementary Figure 3. UV/Vis absorption in $CHCl_3$: $\lambda_{0\text{-}0}$ = 526 nm, $\lambda_{0\text{-}1}$ = 490 nm, $\lambda_{0\text{-}2}$ = 460 nm, ε (at 526 nm) = 4.1 × 10^4 M^{-1} cm^{-1}, as shown in Supplementary Figure 4. PL in $CHCl_3$: $\lambda_{PL\ (0\text{-}0)}$ = 548 nm, $\lambda_{PL\ (0\text{-}1)}$ = 586 nm, PLQY = 73%, as shown in Supplementary Figure 4.

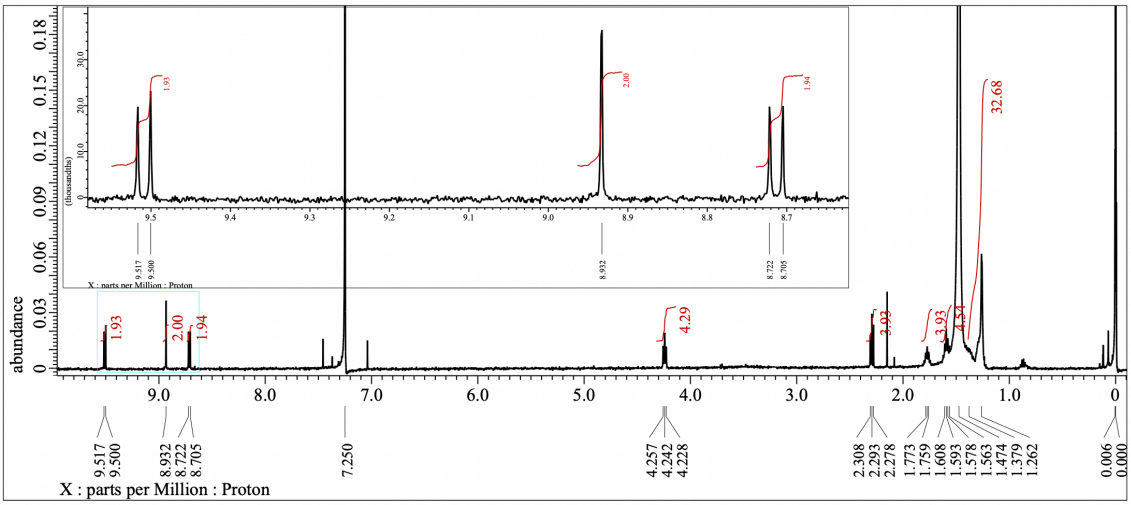

Supplementary Figure 2. ^{1}H NMR spectrum of **PBI$_c$** in $CDCl_3$ at 50 °C.

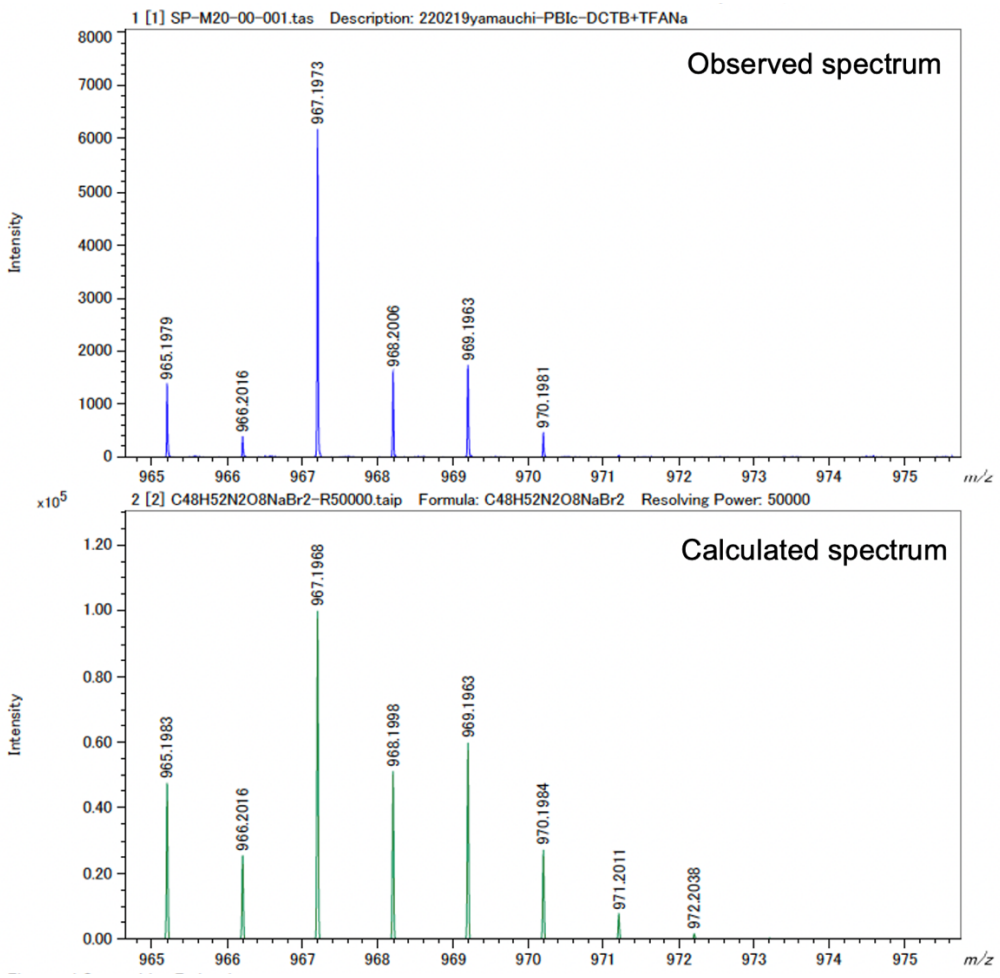

Supplementary Figure 3. HRMS spectrum of **PBI$_c$**.

2-3. Spectroscopic analyses of PBI_c

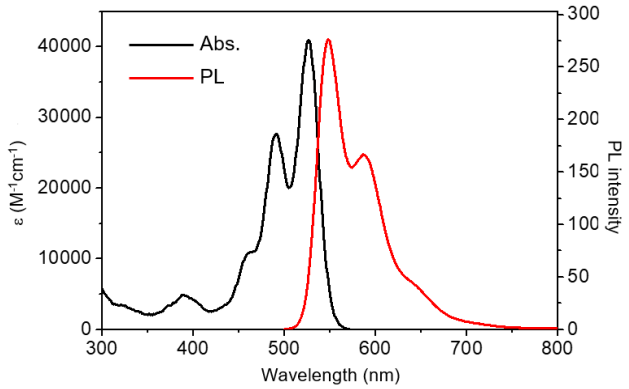

Supplementary Figure 4. UV/Vis absorption (black line) and PL spectra under excitation at 490 nm (red line) of **PBI_c** in $CHCl_3$ ([**PBI_c**] = 4 μM). The sharp absorption spectra and high PLQY indicate that the **PBI_c** exists as a monomer in $CHCl_3$.

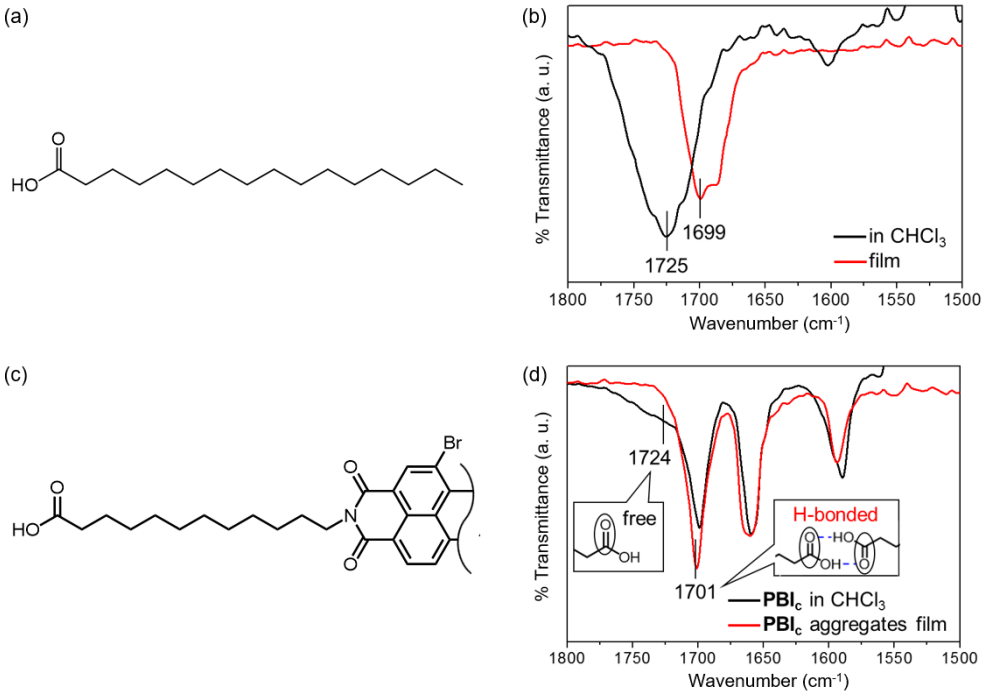

Supplementary Figure 5. (a) Molecular structure of palmitic acid. (b) FTIR spectra of the solution of palmitic acid in $CHCl_3$ (black line, monomers, [palmitic acid] = 1.0 mM)

and that of the dry film of palmitic acid (red line, aggregates). Upon drying the solution of palmitic acid in $CHCl_3$, peaks at 1725 cm^{-1} (free C=O stretching vibration at carboxy groups) shifted to 1699 cm^{-1}. (c) Partial structure of **PBI$_c$**. (d) FTIR spectra of the solution of **PBI$_c$** in $CHCl_3$ (black line, monomers, [**PBI$_c$**] = 600 μM) and that of the **PBI$_c$** aggregates film (red line) which was prepared by drying the solution of **PBI$_c$** aggregates (in $CHCl_3$/cyclohexane (1:9, *v*/*v*)). Upon forming the **PBI$_c$** aggregates, peaks at 1724 cm^{-1} shifted to 1701 cm^{-1}. This spectral change is almost same as a palmitic acid, suggesting the formation of hydrogen bonds between carboxy groups.[2] The strong signals at 1700 cm^{-1} and 1660 cm^{-1} and 1590 cm^{-1} indicate C=O stretching vibration at imide group.

2-4. Synthesis and characterization of PBI_a

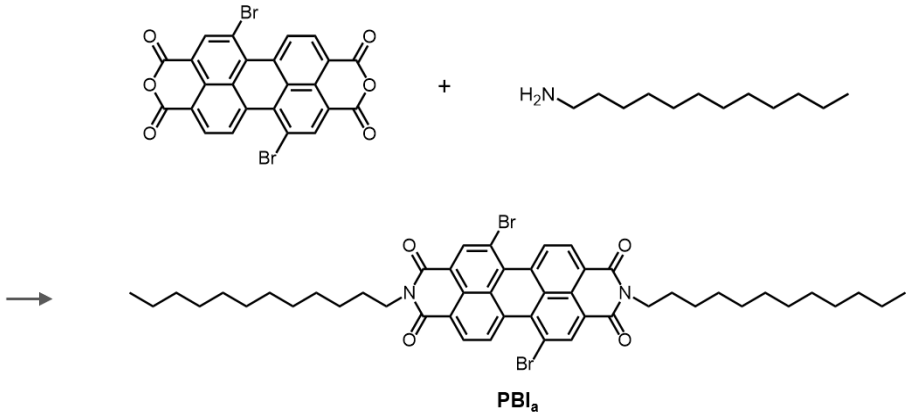

Scheme 2. Synthesis of **PBI_a**. Condition: NMP, toluene, 65 °C, 4 hours.

1,7-Dibromo-3,4,9,10-tetracarboxylic acid dianhydride (100 mg, 0.18 mmol), dodecylamine (74 mg, 0.4 mmol) and *N*-methyl-2-pyrrolidone (NMP, 3 mL) were added to a flask. The mixture was stirred at room temperature for 30 minutes, and then stirred at 65 °C for another 60 minutes. After that, toluene (1 mL) was added into the solution and the reaction mixture was stirred for 3 hours at 65 °C. After cooling, methanol (10 mL) was added into the reaction mixture, and the resulting suspension was separated by centrifugation (15000 rpm, 10 min, 25 °C). The resulting dark red solid was purified by column chromatography on silica gel ($CHCl_3$:hexane = 2:1, Rf = 0.44) and reprecipitated ($CHCl_3$/methanol) to give **PBI_a** (63 mg, 39% yield).

^{1}H NMR (500 MHz, $CDCl_3$, 20 °C): δ (ppm) = 9.50 (d, J = 8.1 Hz, 2H), 8.93 (s, 2H), 8.72 (d, J = 8.2 Hz, 2H), 4.21 (t, J = 7.5 Hz, 4H), 1.78–1.72 (m, 4H), 1.45–1.26 (m, 36H), 0.88 (t, J = 6.8 Hz, 6H), as shown in Supplementary Figure 6. ^{13}C NMR (126 MHz, $CDCl_3$, 20 °C): δ (ppm) = 162.85, 162.34, 138.00, 132.87, 132.72, 129.99, 129.15, 128.46, 126.89, 123.17, 122.73, 120.85, 40.92, 32.02, 29.73, 29.65, 29.46, 27.20, 22.79,

14,24, as shown in Supplementary Figure 7. HRMS (MALDI-TOF, DCTB matrix, TFANa): *m*/*z* [M^+] calcd for $C_{48}H_{56}Br_2N_2O_4$ 882.2601, observed 882.2614, as shown in Supplementary Figure 8. UV/Vis absorption in $CHCl_3$: $\lambda_{0\text{-}0}$ = 526 nm, $\lambda_{0\text{-}1}$ = 490 nm, $\lambda_{0\text{-}2}$ = 460 nm, ε (at 526 nm) = 6.8 × 10^4 M^{-1} cm^{-1}. PL in $CHCl_3$: $\lambda_{PL\ (0\text{-}0)}$ = 548 nm, $\lambda_{PL\ (0\text{-}1)}$ = 586 nm, PLQY = 78%

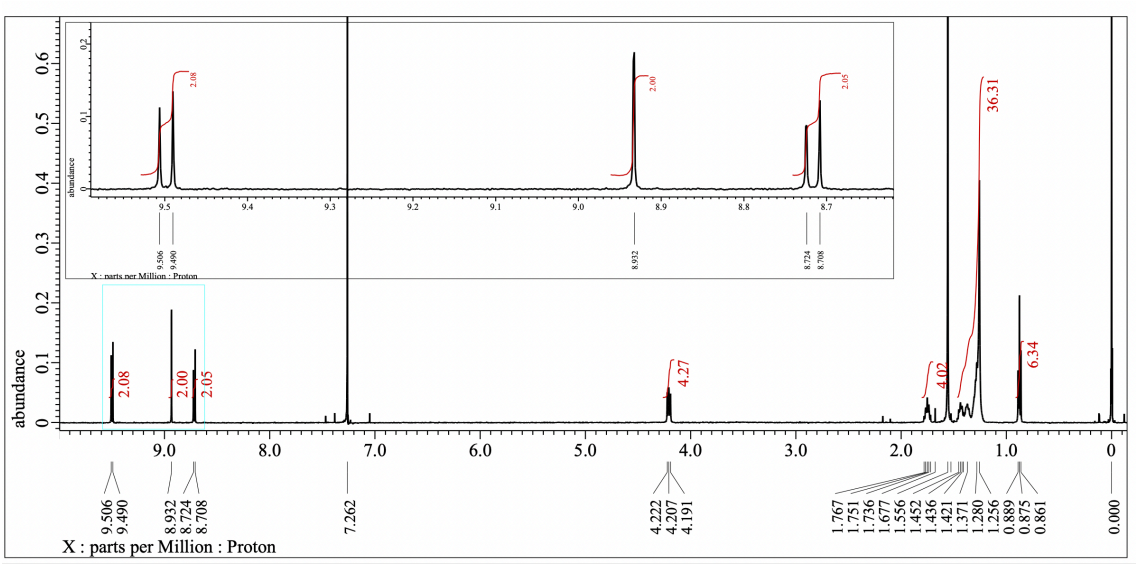

Supplementary Figure 6. ^{1}H NMR spectrum of **PBI$_a$** in $CDCl_3$ at 20 °C.

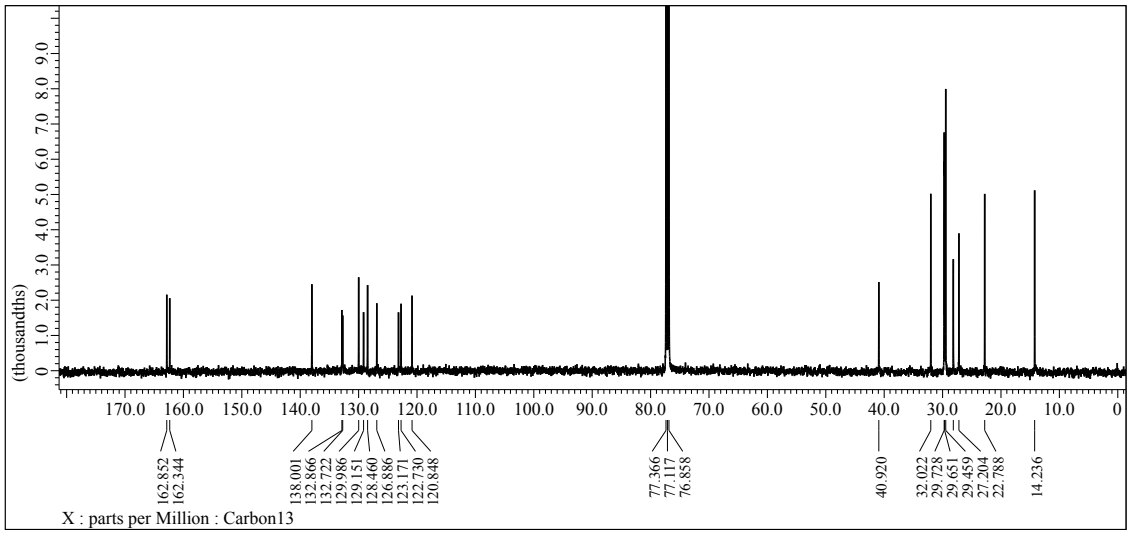

Supplementary Figure 7. ^{13}C NMR spectrum of **PBI$_a$** in $CDCl_3$ at 20 °C.

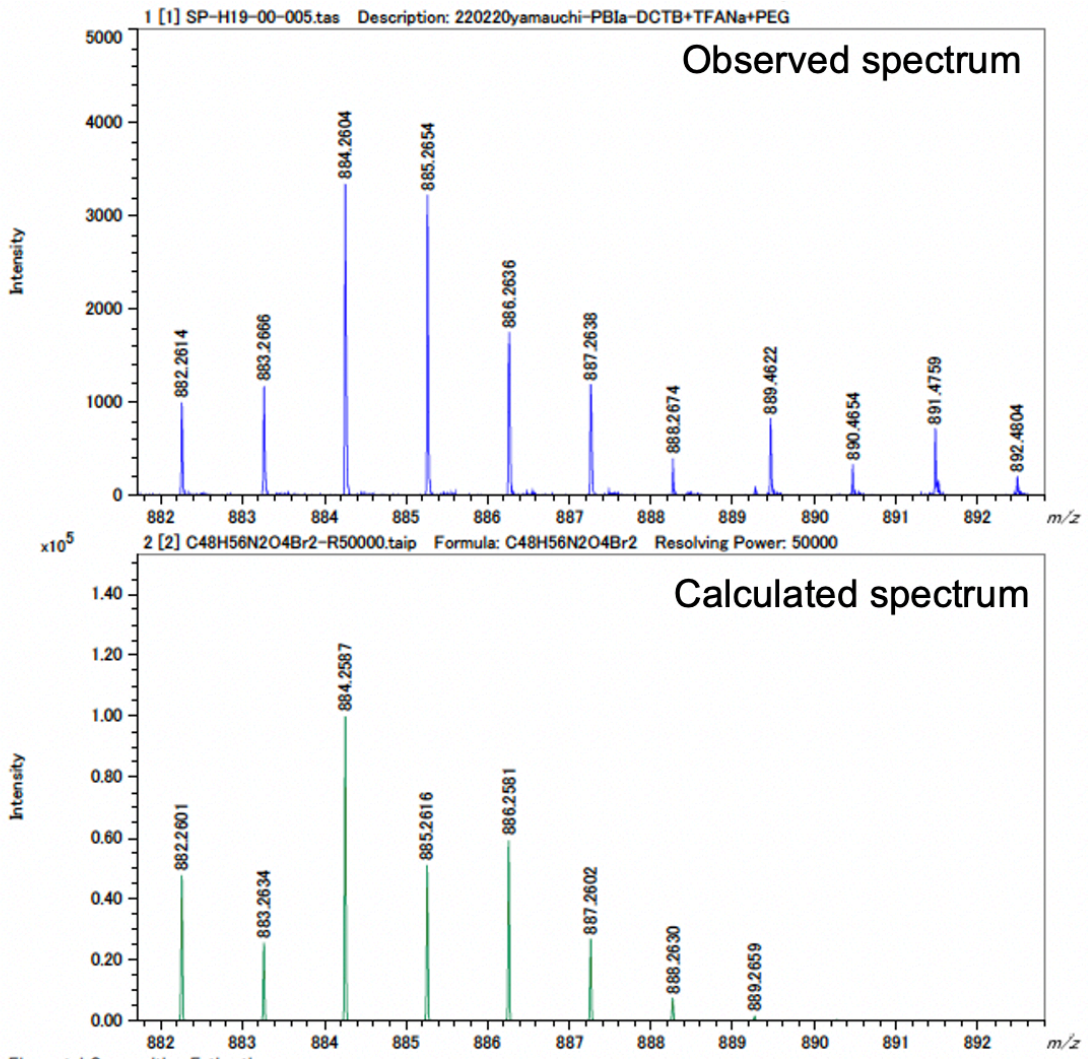

Supplementary Figure 8. HRMS spectrum of **PBI$_a$**.

3. Synthesis and Characterization of NC

Chemicals: Cesium carbonate (Cs_2CO_3, reagent Plus, 99%), lead(II) bromide ($PbBr_2$, 99.999% trace metals basis), toluene (anhydrous, 99.5%), octadecene (ODE, technical grade, 90%), oleylamine (OLA, 70%), and oleic acid (OA, 90%) were purchased from Sigma-Aldrich. All chemicals were used without any further purification.

3-1. Synthesis of $CsPbBr_3$ perovskite NCs

$CsPbBr_3$ perovskite NCs were synthesized following the reported procedure by Protesescu et al. with some minor modification.[3] Briefly, Cs_2CO_3 (0.16 g, 0.50 mmol), OA (0.5 mL), and ODE (8 mL) were loaded into a three-necked round-bottom flask, dried/degassed for 1 h at 120 °C under vacuum, and then stirred under a nitrogen atmosphere at 160 °C until all Cs_2CO_3 dissolved. This resulting clear solution was referred to as Cs-oleate solution. $PbBr_2$ (0.069 g, 0.19 mmol), OA (0.6 mL), OLA (0.6 mL), and ODE (5 mL) were loaded into another three-necked round-bottom flask, dried/degassed under vacuum at 120 °C for 1 h, and then heated under nitrogen gas to 160 °C. After complete dissolution of the $PbBr_2$, the temperature was adjusted at 160 °C, and the Cs-oleate solution (0.4 mL) was swiftly injected. Five seconds after the injection, the reacted solution was quickly cooled down to room temperature with an ice-water bath. The crude solution of the synthesized $CsPbBr_3$ perovskite NC was first centrifuged at 10000 rpm for 3 min at 25 °C to remove the unreacted compounds. The precipitate was dispersed in toluene and then centrifuged at 10000 rpm for 30 min at 25 °C. After centrifugation, the supernatant was collected and used for the measurement. The resulting solutions were stored in the dark at 25 °C.

UV/Vis absorption in toluene: λ (first peak) = 498 nm, D_{UV} = 7.1 nm, ε (at 400 nm) = 7.0×10^6 $M^{-1}cm^{-1}$.[4] PL in toluene: λ_{max} = 508 nm, FWHM = 21 nm, PLQY = 47%. TEM: D_{TEM} = 8.0 ± 0.9 nm, as shown in Supplementary Figure 9.

3-2. Spectroscopic and microscopic analyses of NCs

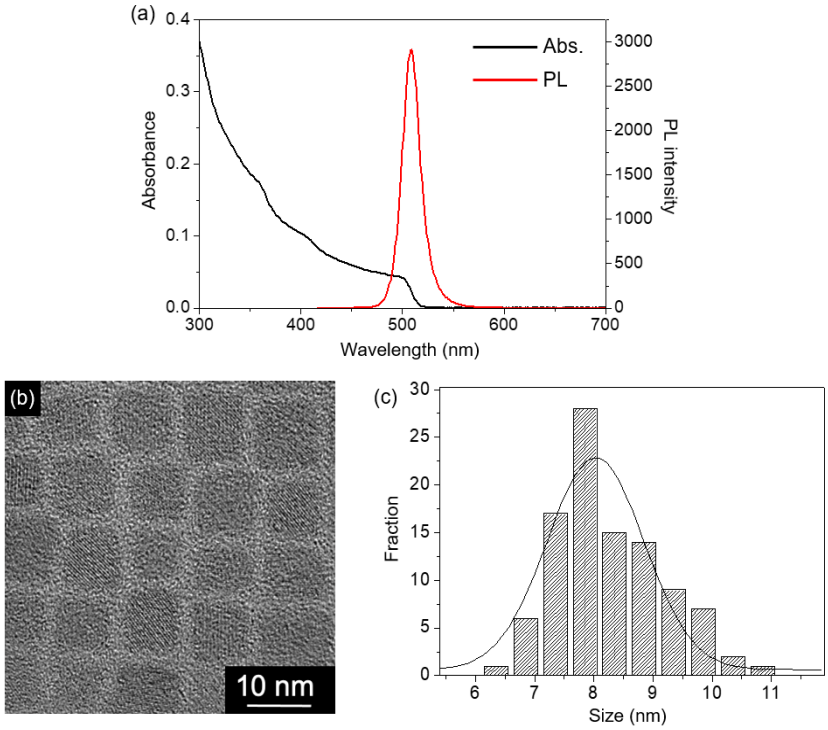

Supplementary Figure 9. (a) UV/Vis absorption and PL spectra under excitation at 405 nm of **NC** in toluene ([**NC**] = 0.01 μM). (b) TEM image of **NC**s spin-coated from solution onto a carbon-coated Cu grid. (c) Size distribution of **NC** obtained from TEM images.

3-3. Absorption spectrum of redispersed NCs

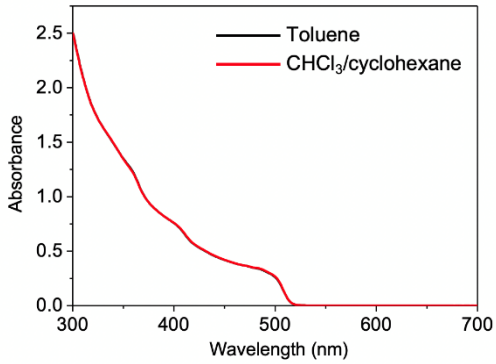

Supplementary Figure 10. Change in absorption of the solution of **NC** by changing the solvent from toluene to $CHCl_3$/cyclohexane (1:9, *v*/*v*) via dry film of **NC**.

4. Supplementary Figures and Tables

4-1. Tyndall effect in the solution of PBI_c aggregates

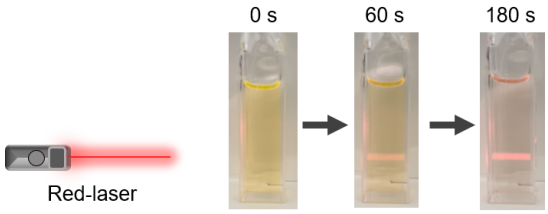

Supplementary Figure 11. The observation of Tyndall effect under red-laser irradiation (635 nm) of the **PBI_c** solution in $CHCl_3$/cyclohexane (1:9, *v*/*v*) over time.

4-2. AFM analyses of PBI_c aggregates

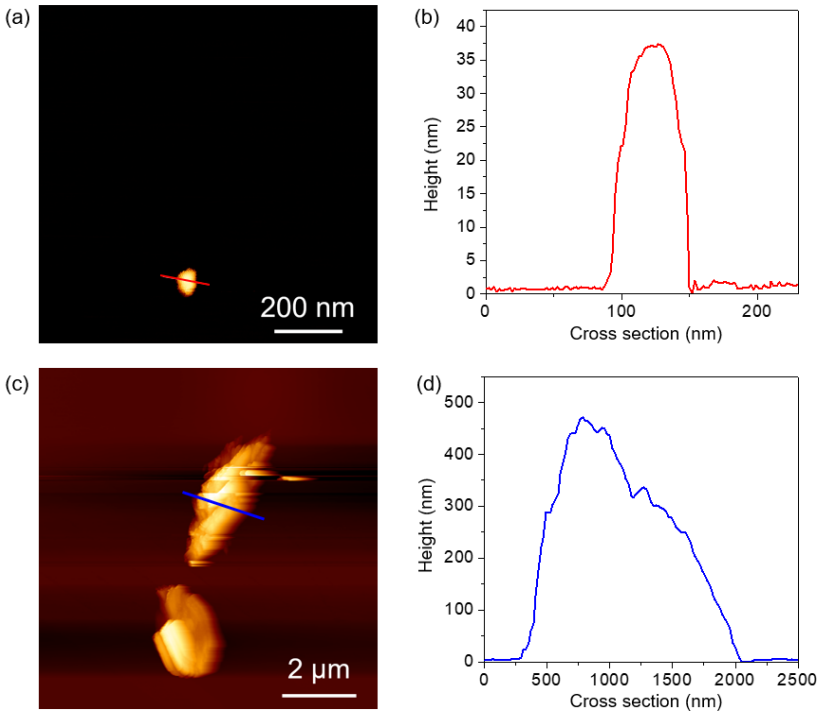

Supplementary Figure 12. AFM images of the **PBI_c** aggregates that formed in $CHCl_3$/cyclohexane (1:9, *v*/*v*) at t_{aging} = 60 s (a) and 180 s (c). (b,d) The cross-sectional analysis along the lines in (a) and (c).

4-3. Tyndall effect in the solution of NC-PBI$_c$

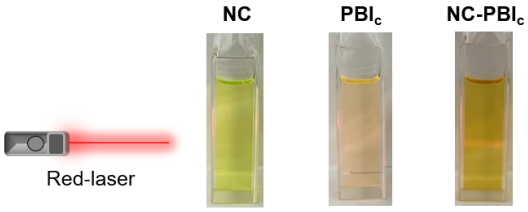

Supplementary Figure 13. The observation of Tyndall effect under red-laser irradiation (635 nm) of the **NC** solution ([**NC**] = 0.1 μM, in $CHCl_3$), **PBI$_c$** monomer solution ([**PBI$_c$**] = 10 μM, in $CHCl_3$) and **NC-PBI$_c$** solution ([**NC**] = 0.1 μM, [**PBI$_c$**] = 10 μM, in $CHCl_3$).

4-4. TEM images of NC-PBI$_c$

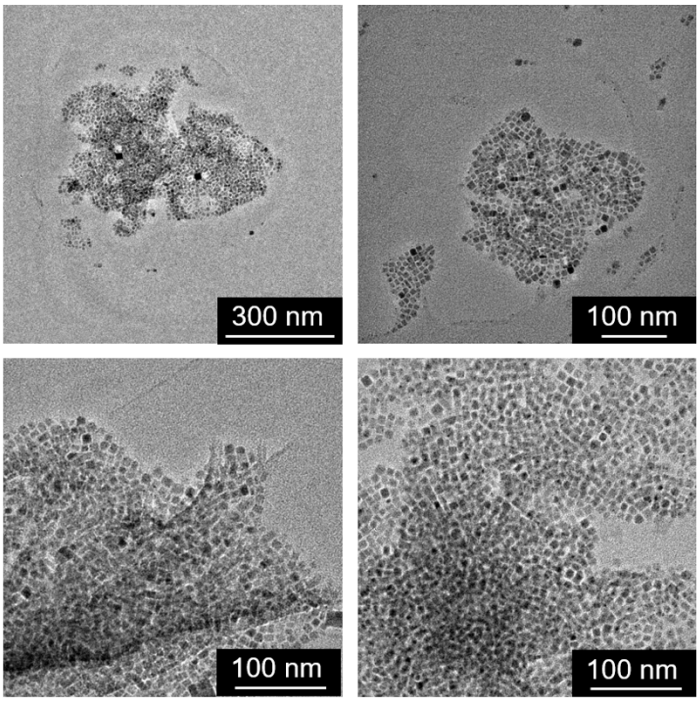

Supplementary Figure 14. TEM images of **NC-PBI$_c$** ([**NC**] = 0.1 μM, [**PBI$_c$**] = 10 μM, in $CHCl_3$) immediately after mixing.

4-5. TEM images of sole NCs

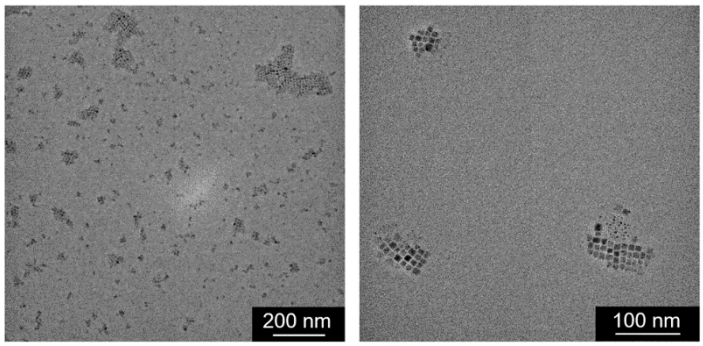

Supplementary Figure 15. TEM images of **NC** ([**NC**] = 0.1 μM, in $CHCl_3$/cyclohexane (1:9, *v*/*v*)).

4-6. XRD patterns of NC and coaggregates

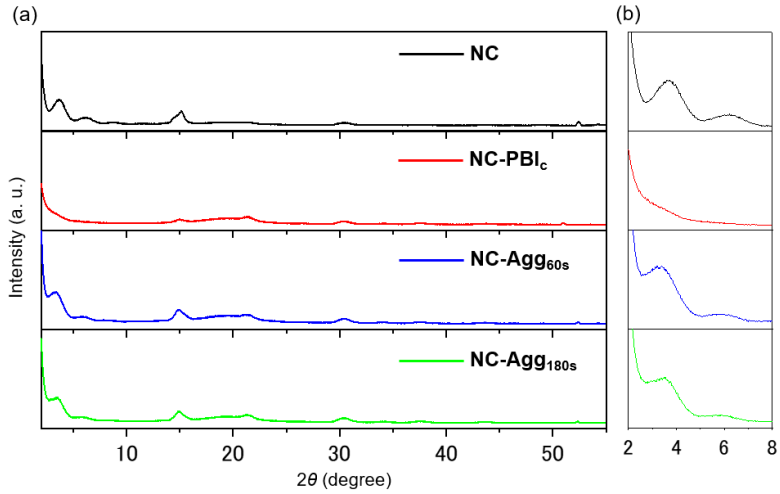

Supplementary Figure 16. (a) XRD patterns of aggregated **NC**s and coaggregates (**NC-PBI$_c$**, **NC-Agg$_{60s}$** and **NC-Agg$_{180s}$**). (b) Expanded view of the peaks at $2\theta \sim 8°$ in (a).

4-7. TEM images of NC-PBI$_a$

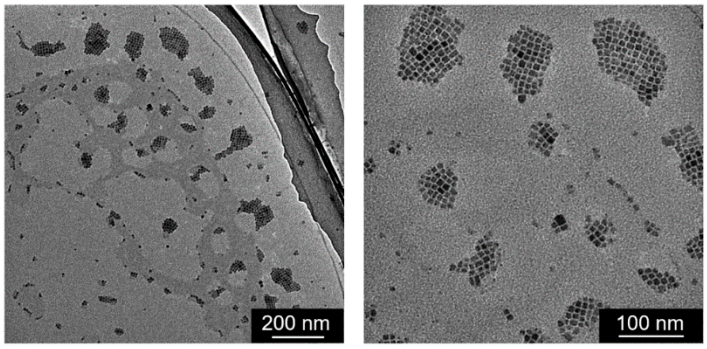

Supplementary Figure 17. TEM images of **NC-PBI$_a$** ([**NC**] = 0.1 μM, [**PBI$_a$**] = 10 μM, in $CHCl_3$) immediately after mixing.

4-8. Absorption spectra of coaggregates

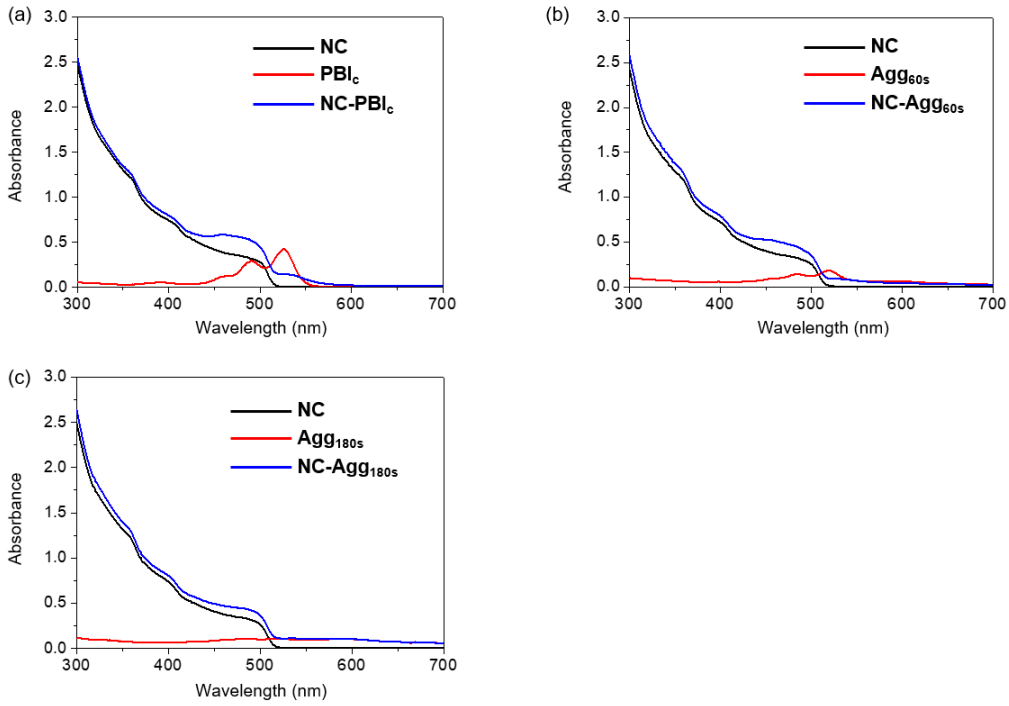

Supplementary Figure 18. UV/Vis absorption spectra of **NC-PBI$_c$** (a) and **NC-Agg$_{60s}$** (b) and **NC-Agg$_{180s}$** (c). The UV/Vis absorption spectrum of the sole **NC** ([**NC**] = 0.1 μM, black line), **PBI$_c$** monomer, **Agg$_{60s}$** and **Agg$_{180s}$** ([**PBI$_c$**] = 10 μM, red line) are shown for comparison, respectively.

4-9. TEM images of NC-Agg$_{60s}$

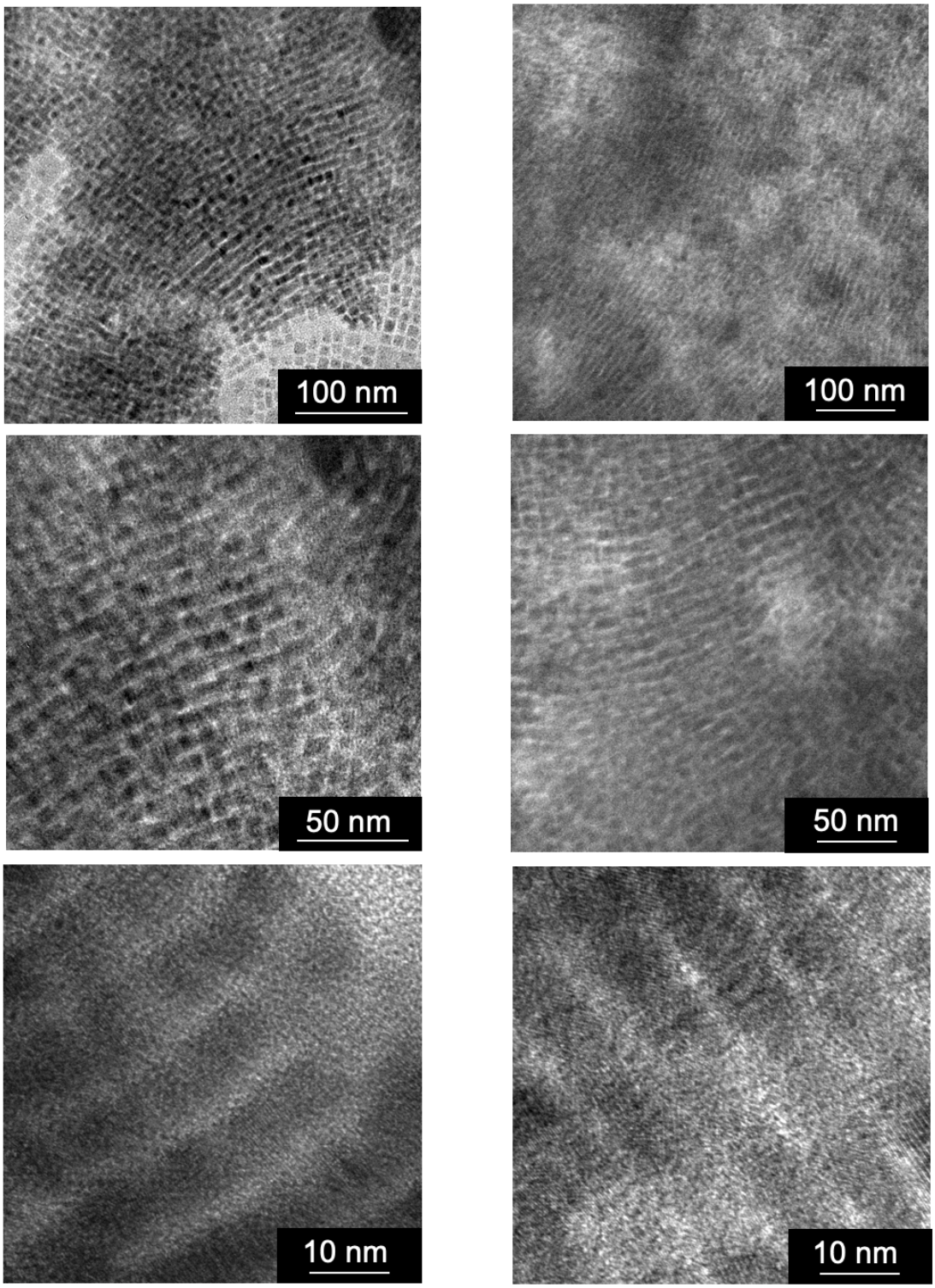

Supplementary Figure 19. TEM images of **NC-Agg$_{60s}$** ([**NC**] = 0.1 μM, [**PBI$_c$**] = 10 μM, in $CHCl_3$/cyclohexane (1:9, *v*/*v*)) immediately after mixing.

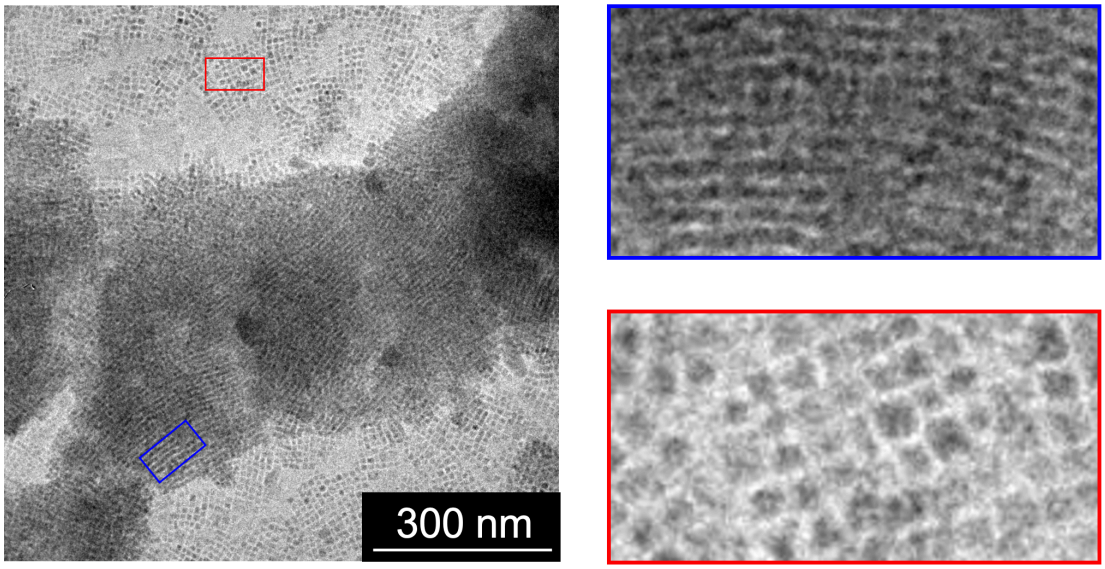

Supplementary Figure 20. Low-magnification TEM image of **NC-Agg$_{60s}$** and their magnified images of the area of a Roman-pavement-like structure (blue square) and the area of isolated **NC**s (red square). The area of a Roman-pavement-like structure is darker than the area of isolated **NC**s, indicating the difference of electron density. Namely, the different contrasts of the TEM image suggest the formation of multilayer structures.

4-10. Spectral change of NC-Agg$_{60s}$ over time

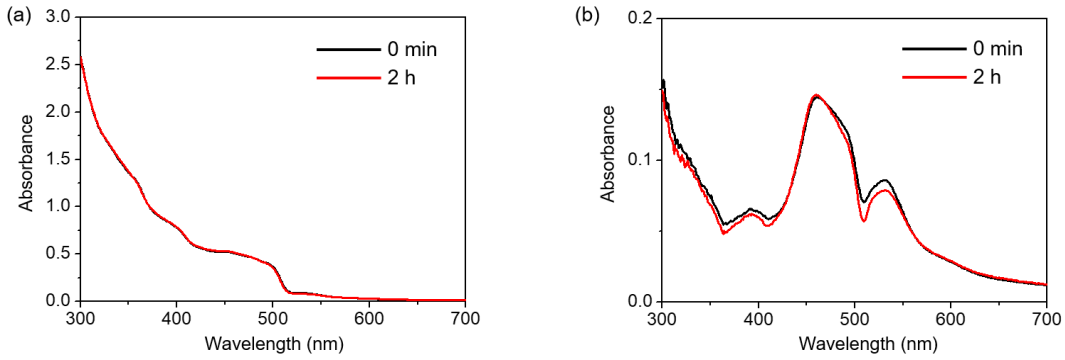

Supplementary Figure 21. Time-changes in UV/Vis absorption spectra of **NC-Agg$_{60s}$** (a) and the difference spectra between **NC-Agg$_{60s}$** and sole **NC** (b).

4-11. TEM images of NC-Agg$_{60s}$ after 2 hours

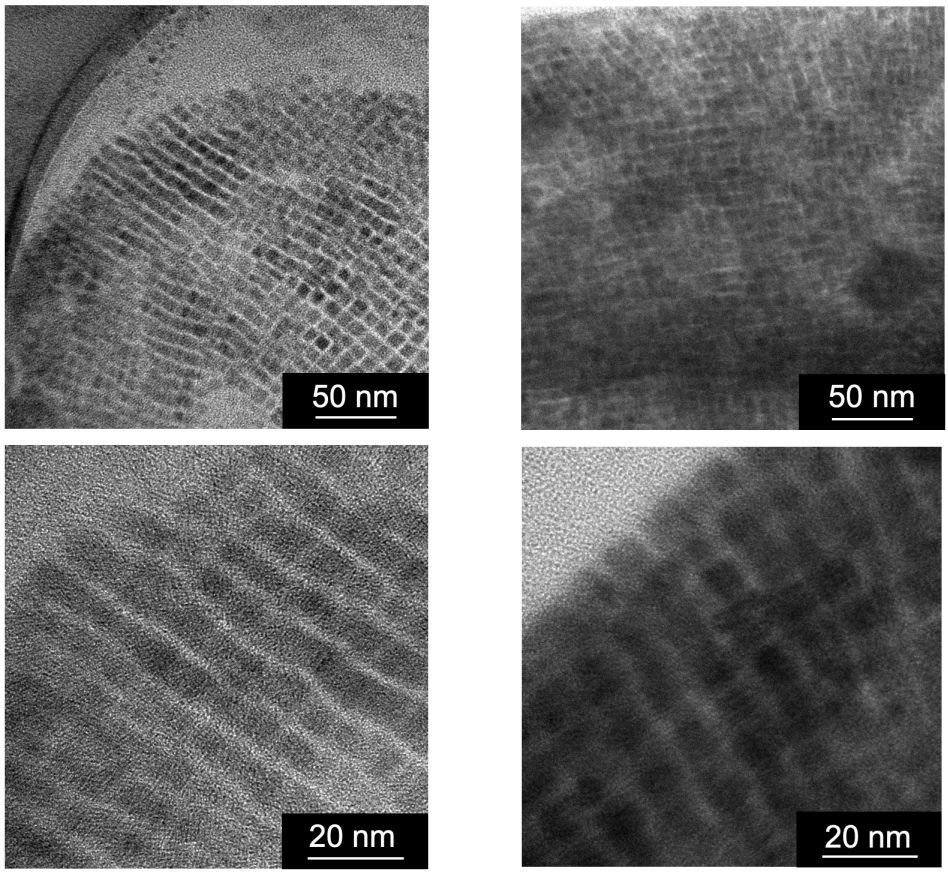

Supplementary Figure 22. TEM images of **NC-Agg$_{60s}$** after 2 hours.

4-12. TEM images of NC-Agg$_{180s}$

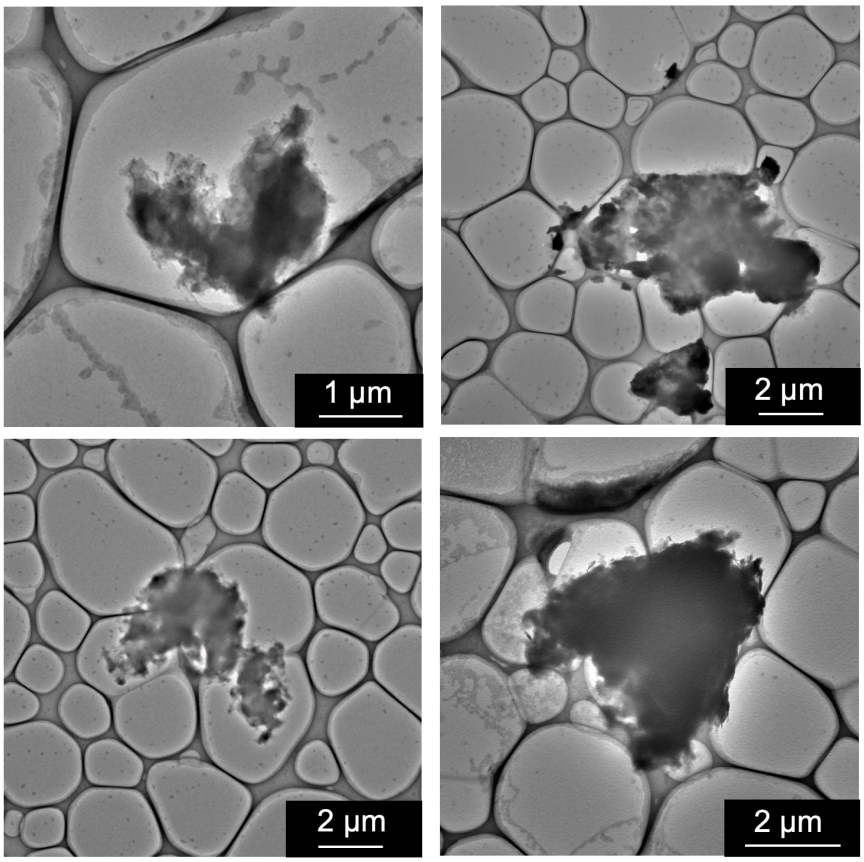

Supplementary Figure 23. TEM images of **NC-Agg$_{180s}$** ([**NC**] = 0.1 μM, [**PBI$_c$**] = 10 μM, in $CHCl_3$/cyclohexane (1:9, *v*/*v*)).

4-13. TEM images of NC-Agg$_{180s}$ at low concentration of NC

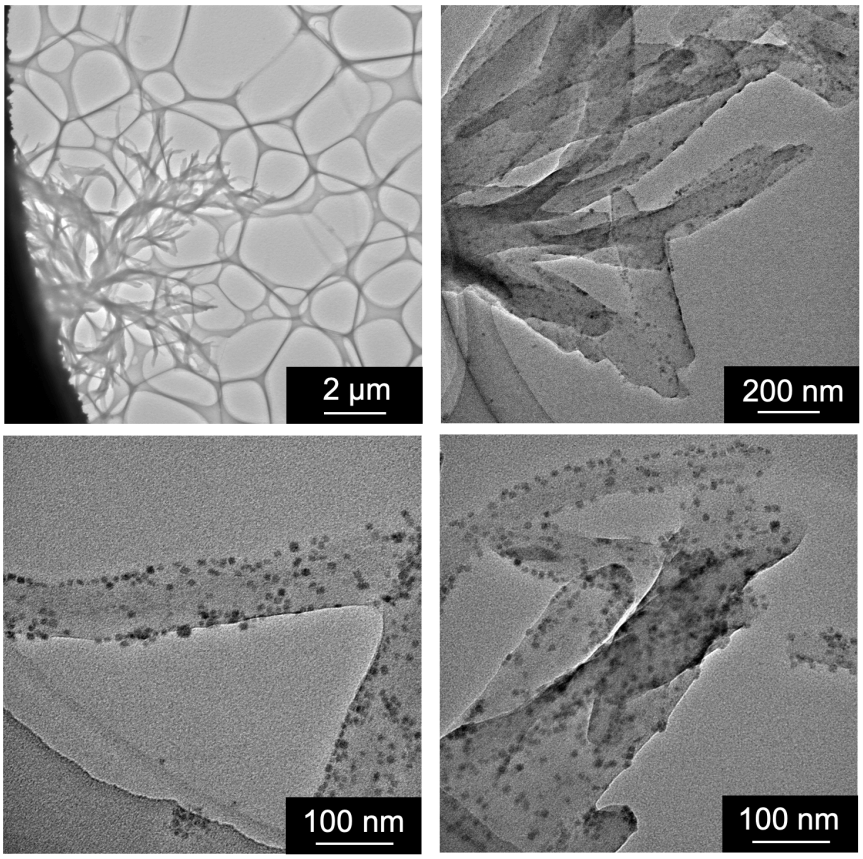

Supplementary Figure 24. TEM images of **NC-Agg$_{180s}$** at low concentration of **NC** ([**NC**] = 0.01 μM, [**PBI$_c$**] = 10 μM, in $CHCl_3$/cyclohexane (1:9, *v*/*v*)).

4-14. Spectral overlap

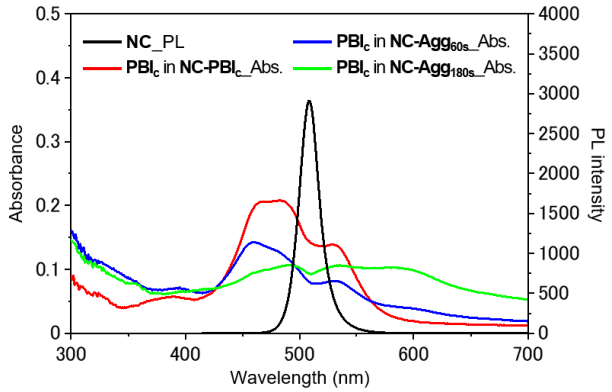

Supplementary Figure 25. UV/Vis absorption spectra of **PBI$_c$** in **NC-PBI$_c$** (red line) or **PBI$_c$** in **NC-Agg$_{60s}$** (blue line) or **PBI$_c$** in **NC-Agg$_{180s}$** (green line) and PL spectrum of the **NC** (black line) in $CHCl_3$/cyclohexane (1:9, *v*/*v*). Based on the spectral overlap equation $J(\lambda) = \oint [F_D(\lambda)*\varepsilon_A(\lambda)*\lambda^4]\,d\lambda$, the **NC**/**PBI$_c$** in **NC-PBI$_c$** and **NC**/**PBI$_c$** in **NC-Agg$_{60s}$** and **NC**/**PBI$_c$** in **NC-Agg$_{180s}$** J values were estimated to be 1.0×10^{15}, 5.8×10^{14} and 6.7×10^{14} $M^{-1}\,cm^{-1}\,nm^4$ respectively. [5, 6]

4-15. Solvent dependence of NC

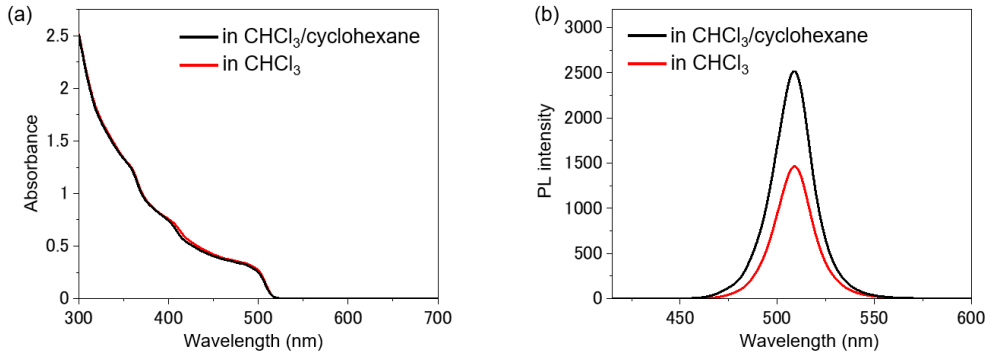

Supplementary Figure 26. UV/Vis absorption spectra (a) and PL spectra under excitation at 405 nm (b) of **NC** in $CHCl_3$/cyclohexane (1:9, *v*/*v*, black line) and in $CHCl_3$ (red line) ([**NC**] = 0.1 μM).

4-16. Absorption ratio of NC and PBI_c in coaggregates

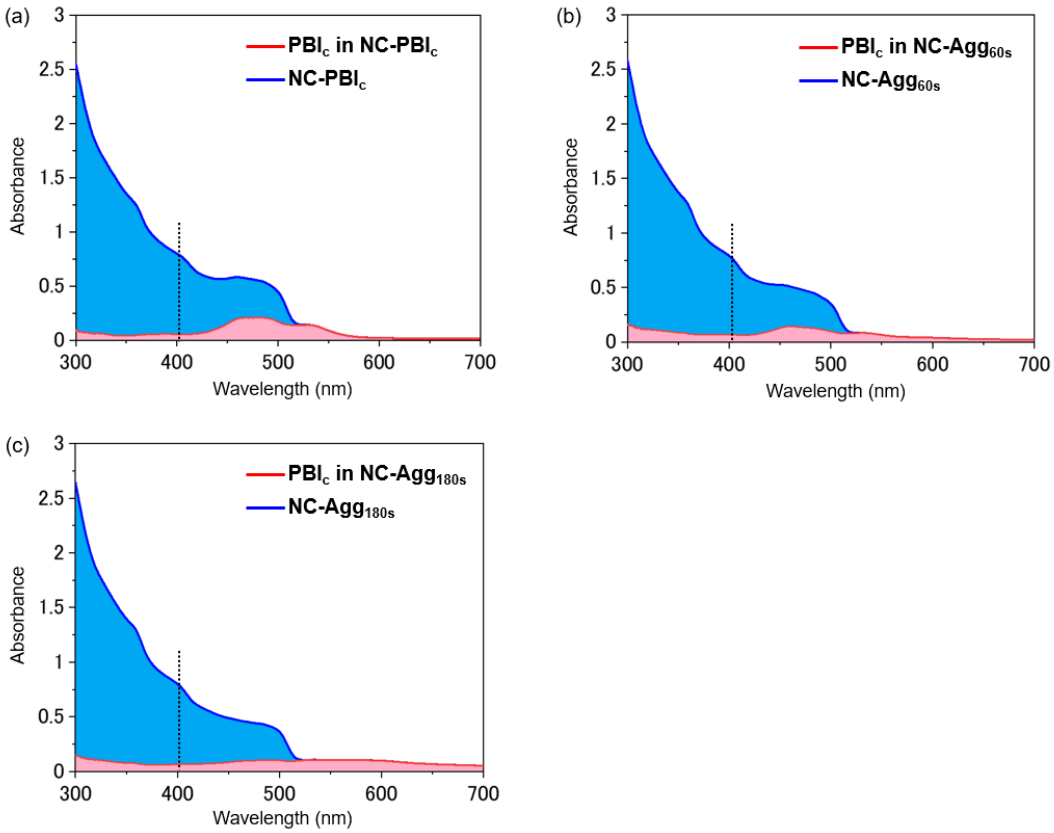

Supplementary Figure 27. (a–c) UV/Vis absorption spectra of coaggregates (**NC-PBI_c** (a), **NC-Agg_{60s}** (b), **NC-Agg_{180s}** (c), blue line) and **PBI_c** in each coaggregates (red line). The dashed line shows the absorption ratio of **PBI_c** and **NC** in coaggregates at 405 nm.

4-17. PL decay curves corresponding to PL of NC

Supplementary Table 1. The fitting parameters estimated from the PL decay curves of solution of **NCs** in $CHCl_3$/cyclohexane (1:9, *v*/*v*) and dry film of **NC**, spin-coated coaggregates film (**NC-Agg$_{60s}$** and **NC-Agg$_{180s}$**) shown in Figure 7d and Supplementary Fig. 28. These PL decay curves corresponding to the PL of **NC** in the range of 450–500 nm using band-pass filter. The PL decay curves were fitted by the sum of three-exponential functions, $I(t) = \alpha_1\exp(-t/\tau_1) + \alpha_2\exp(-t/\tau_2) + \alpha_3\exp(-t/\tau_3)$, where τ and α are the PL lifetime and the normalized amplitude, respectively.

	τ_1 (ns)	α_1 (%)	τ_2 (ns)	α_2 (%)	τ_3 (ns)	α_3 (%)	τ_{ave} (ns)
NC in $CHCl_3$/cyclohexane	1.2	29.7	3.8	59.8	9.2	10.5	3.6
NC film (No.1 in Fig.28)	1.0	16.7	3.4	70.0	6.0	13.4	3.3
NC-Agg$_{60s}$	0.5	79.8	1.6	18.3	6.8	1.9	0.8
NC-Agg$_{180s}$	0.4	55.0	1.3	41.0	4.1	4.0	0.9

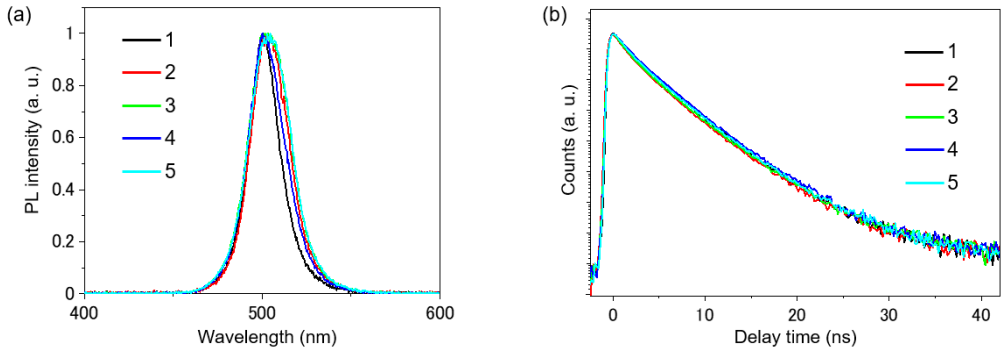

Supplementary Figure 28. (a) PL spectra of dry film of **NC** (λ_{ex} = 405 nm). (b) PL decay curves corresponding to PL in the range of 450–500 nm in dry film of **NC** (λ_{ex} = 405 nm). The **NC** film was prepared by drop-casting from the solution ([**NC**] = 0.1 μM, in $CHCl_3$/cyclohexane (1:9, *v*/*v*)) onto a glass substrate.

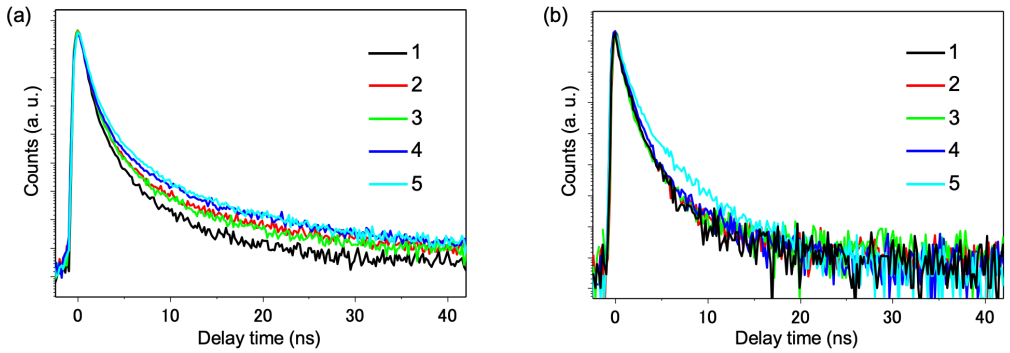

Supplementary Figure 29. (a,b) PL decay curves (λ_{ex} = 405 nm) corresponding to the PL of **NC** in **NC-Agg$_{60s}$** (a) and **NC-Agg$_{180s}$** (b) in the range of 450–500 nm, spin-coated from the solution onto a hydrophobic substrate.

Supplementary Table 2. The fitting parameters estimated from the PL decay curves of spin-coated coaggregates film (**NC-Agg$_{60s}$** (a), **NC-Agg$_{180s}$** (b)) shown in Supplementary Fig. 29. These PL decay curves corresponding to the PL of **NC** in the range of 450–500 nm using band-pass filter. The PL decay curves were fitted by the sum of three-exponential functions.

(a)

No.	τ_1 (ns)	α_1 (%)	τ_2 (ns)	α_2 (%)	τ_3 (ns)	α_3 (%)	τ_{ave} (ns)
1	0.6	75.9	1.9	21.2	7.1	2.8	1.1
2	0.6	78.6	1.7	19.7	7.9	1.7	0.9
3	0.6	79.3	1.8	18.8	7.3	1.9	1.0
4	0.6	80.0	1.8	18.0	7.7	2.0	0.9
5	0.7	77.4	2.0	20.4	8.4	2.3	1.1

(b)

No.	τ_1 (ns)	α_1 (%)	τ_2 (ns)	α_2 (%)	τ_3 (ns)	α_3 (%)	τ_{ave} (ns)
1	0.6	53.3	1.4	44.2	4.3	2.5	1.0
2	0.4	56.8	1.2	39.8	4.0	3.4	0.8
3	0.4	65.0	1.1	32.1	3.5	2.9	0.7
4	0.5	44.0	1.3	53.4	5.6	2.6	1.0
5	0.5	42.7	1.3	50.6	4.3	6.7	1.2

4-18. PL decay curves corresponding to PL of PBI_c

Supplementary Table 3. The fitting parameters estimated from the PL decay curves of dry film of **PBI_c** aggregates and spin-coated coaggregates film (**NC-Agg_{60s}**, **NC-Agg_{180s}**) shown in Figure 7e. These PL decay curves corresponding to the PL of **PBI_c** in the range of 593–880 nm using long-pass filter. The PL decay curves were fitted by the sum of two or three-exponential functions.

	τ_1 (ns)	α_1 (%)	τ_2 (ns)	α_2 (%)	τ_3 (ns)	α_3 (%)	τ_{ave} (ns)
PBI_c aggregates	0.6	91.6	1.3	8.4	-	-	0.6
NC-Agg_{60s}	0.5	83.5	1.2	14.1	5.5	2.4	0.7
NC-Agg_{180s}	0.5	92.3	1.3	7.7	-	-	0.6

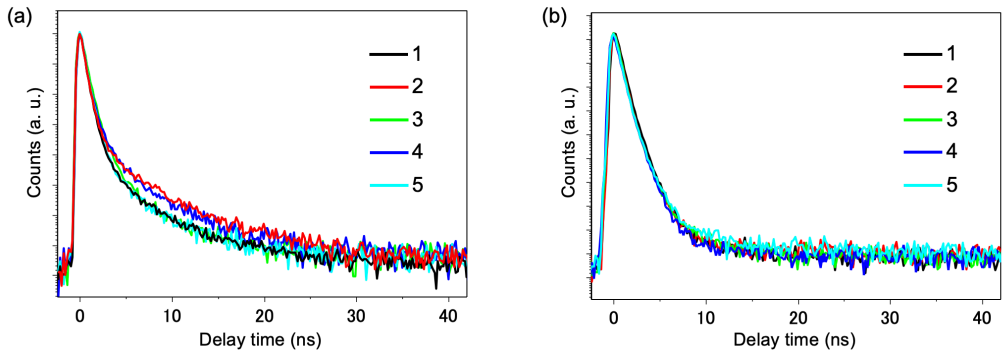

Supplementary Figure 30. (a,b) PL decay curves (λ_{ex} = 405 nm) corresponding to the PL of **PBI_c** in **NC-Agg_{60s}** (a) and **NC-Agg_{180s}** (b) in the range of 593–880 nm, spin-coated from the solution onto a hydrophobic substrate.

Supplementary Table 4. The fitting parameters estimated from the PL decay curves of spin-coated coaggregates film (**NC-Agg$_{60s}$** (a), **NC-Agg$_{180s}$** (b)) shown in Supplementary Fig. 30. These PL decay curves corresponding to the PL of **PBI$_c$** in the range of 593–880 nm using long-pass filter. The PL decay curves were fitted by the sum of two or three-exponential functions.

(a)

No.	τ_1 (ns)	α_1 (%)	τ_2 (ns)	α_2 (%)	τ_3 (ns)	α_3 (%)	τ_{ave} (ns)
1	0.5	78.1	1.1	20.1	5.2	1.8	0.7
2	0.5	86.8	1.6	10.3	6.4	3.0	0.8
3	0.5	74.7	1.1	24.1	4.8	1.2	0.7
4	0.4	66.8	1.1	29.6	5.0	3.6	0.8
5	0.5	82.2	1.0	16.5	4.7	1.3	0.6

(b)

No.	τ_1 (ns)	α_1 (%)	τ_2 (ns)	α_2 (%)	τ_3 (ns)	α_3 (%)	τ_{ave} (ns)
1	0.6	89.5	1.2	10.5	-	-	0.6
2	0.5	90.6	1.3	9.4	-	-	0.6
3	0.5	93.5	1.4	6.5	-	-	0.6
4	0.6	89.9	1.2	10.1	-	-	0.6
5	0.5	90.7	1.2	9.3	-	-	0.6

References

1. Kang, R. *et al.* Tuning the formation of reductive species of perylene-bisimide derivatives in DMF via aggregation matter. *Chem. Commun.* **53**, 10018-10021 (2017).
2. Helmers, I., Shen, B., Kartha, K. K., Albuquerque, R. Q., Lee, M., Fernandez, G. Impact of Positional Isomerism on Pathway Complexity in Aqueous Media. *Angew. Chem. Int. Ed.* **59**, 5675-5682 (2020).
3. Protesescu, L. *et al.* Nanocrystals of Cesium Lead Halide Perovskites (CsPbX(3), X = Cl, Br, and I): Novel Optoelectronic Materials Showing Bright Emission with Wide Color Gamut. *Nano Lett.* **15**, 3692-3696 (2015).
4. Maes, J. *et al.* Light Absorption Coefficient of CsPbBr3 Perovskite Nanocrystals. *J. Phys. Chem. Lett.* **9**, 3093-3097 (2018).
5. Goldman, E. R. *et al.* A hybrid quantum dot-antibody fragment fluorescence resonance energy transfer-based TNT sensor. *J. Am. Chem. Soc.* **127**, 6744-6751 (2005).
6. Lakowicz, J. Principles of Fluorescence Spectroscopy. *Springer, New York* XXVI, 954 (2006).